JOURNAL OF CHEMICAL INFORMATION AND MODELING

Article

pubs.acs.org/jcim

Study of *E/Z* Isomerization in a Series of Novel Non-ligand Binding Pocket Androgen Receptor Antagonists

Fernando Blanco,*[,†] Billy Egan,[‡] Laura Caboni,[†] José Elguero,[§] John O'Brien,[⊥] Thomas McCabe,[⊥] Darren Fayne,[†] Mary J. Meegan,[‡] and David G. Lloyd*[,†]

[†]Molecular Design Group, School of Biochemistry and Immunology, and [‡]School of Pharmacy and Pharmaceutical Sciences, Trinity Biomedical Science Institute, and [⊥]School of Chemistry, Trinity College Dublin, Dublin 2, Ireland

[§]Instituto de Química Médica, CSIC, Juan de la Cierva, 3, E-28006 Madrid, Spain

Supporting Information

ABSTRACT: We report the conformational analysis of a series of 3-hydroxy-*N*′-((naphthalen-2-yl)methylene)naphthalene-2-carbohydrazides. This class of compounds has recently been reported as androgen receptor (AR)-coactivator disruptors for potential application in prostate cancer therapy. Definition of the *E/Z* isomerism around the imine linker group (hydrazide) is significant from a mechanistic point of view. A detailed study using theoretical calculations coupled with experimental techniques has allowed us determine an initial preference for the *E* isomer. The biological activity of newly synthesized compounds at the androgen receptor, along with a series of structural analogs, was determined and provides the basis for preliminary qualitative structure−activity relationship analysis.

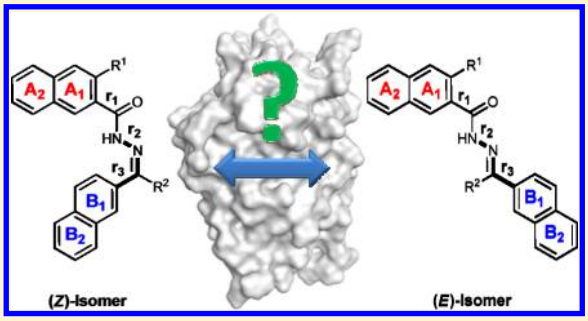

1. INTRODUCTION

In a recent study, we demonstrated the activity of members of the 3-hydroxy-*N*′-((naphthalen-2-yl)methylene)naphthalene-2-carbohydrazide family as novel androgen receptor (AR) antagonists and their potential application in prostate cancer therapy.[1] AR is a member of the highly homologous family of steroidal nuclear receptors (NRs) that regulate transcription of target genes in a ligand dependent fashion.[2] NRs are composed of a modular structure including an *N*-terminal domain (NTD), a DNA binding domain (DBD), and a ligand binding domain (LBD) which encloses a central ligand binding pocket (LBP) where endogenous hormones bind.[3] These include testosterone (Tes) and dihydrotestosterone (DHT) in the specific case of AR. Antiandrogens, in a pharmaceutical setting, typically act by displacing the natural hormones from the LBP; however, acquired drug resistance after prolonged use is a major concern which impairs their application in advanced stages of prostate cancer. The ligands we recently reported[1] function via an alternative non-LBP mediated mechanism which targets AR association with coactivators. Coactivators are essential for AR activity as transcription factors, and the direct disruption of this interaction can potentially overcome therapeutic liabilities of solely targeting the LBP. All of these compounds share the presence of an *N*-acylhydrazone linker, which can exist in two different *E/Z* isomeric forms. Characterization of the *E/Z* isomerism around the linker is substantial for the elucidation of the most probable bioactive conformation in the interaction with the target.

The first systematic studies of the *E/Z* isomerism of hydrazones were carried out by Karabatsos.[4−14] Other studies are summarized in Scheme 1.

Scheme 1. Previously Studied Hydrazone Family Members

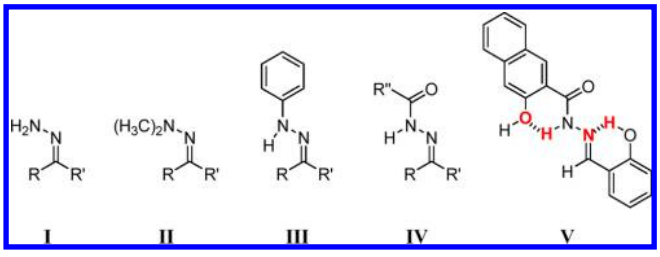

The simpler hydrazones (**I**, N−NH_2) were studied by Minabe,[15] Lemal,[16] and Alkorta.[17] *N,N*-Dimethyl derivatives (**II**) were reported by Elguero[18] and Lu.[19] *N*-Aryl derivatives, usually *N*-phenyl **III**, are the most common hydrazones.[4−14,20−22] Less frequent, but closely related to the compounds of the present study, are the *N*-acylhydrazones **IV**.[23−26]

The most interesting result, in the context of the present work, is a report on the crystal structure of **V** and the two hydrogen bonds (HB), N−H···O and O−H···N, present in its structure.[27]

Received: June 28, 2012
Published: August 2, 2012

dx.doi.org/10.1021/ci300299n | *J. Chem. Inf. Model.* 2012, 52, 2387−2397

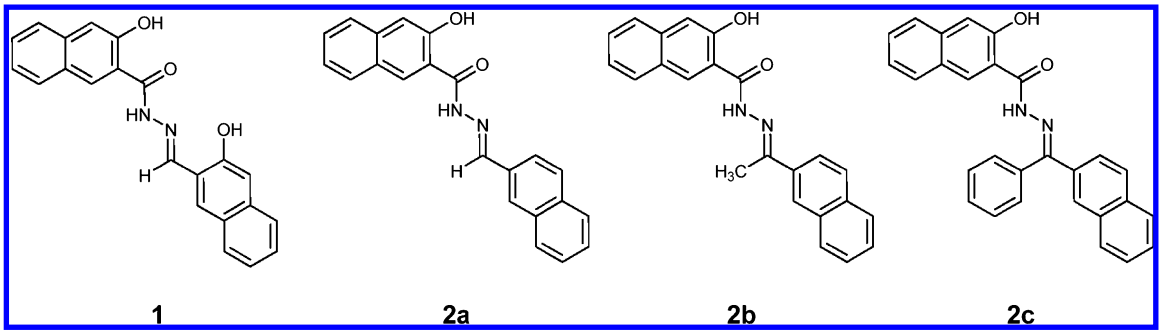

Figure 1. Compounds studied in this work.

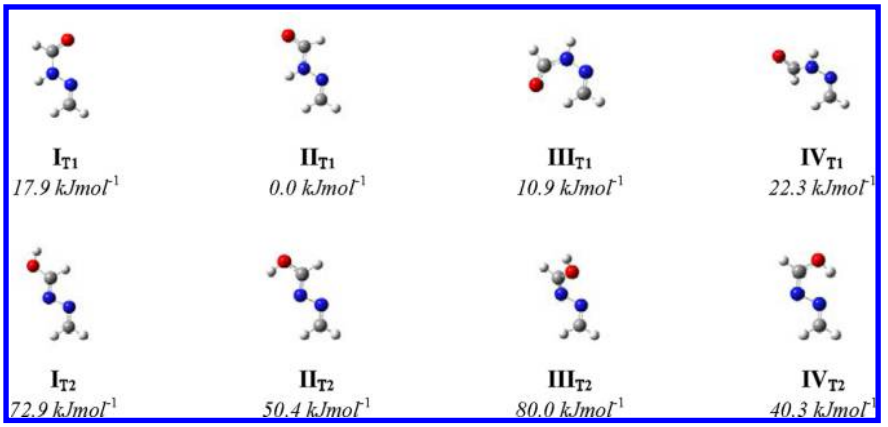

Figure 2. Optimized geometries and relative energies of the *N*-acylhydrazone tautomers/rotamers at the B3LYP/6-311++G** level.

The impact of substitution on the conformational isomerism around the hydrazone and subsequent impact on conformer ratios is of particular interest. In the absence of a protein cocrystallized structure for these compounds, we carried out a conformational study, both theoretical (DFT calculations) and experimental (synthesis, NMR, and X-ray characterization), of the most representative active ligands of the AR non-LBP series, the 3-hydroxy-*N*′-(naphthalen-2-ylmethylene)-2-naphthohydrazide (**1**) and some related systems (**2a**−**c**). Biological and qualitative structure−activity relationship (SAR) analysis of both the studied compounds and some interesting analogs has also been included in the discussion.

2. RESULTS AND DISCUSSION

2.1. Conformational Analysis. A theoretical study of the *E*/*Z* isomerism in a series of 3-hydroxy-*N*′-((naphthalen-2-yl)methylene)naphthalene-2-carbohydrazides (Figure 1) has been performed using DFT calculations.

As an initial approach, we evaluated the tautomeric/conformational geometries of the simple linker (*N*-acylhydrazone) to establish the most favorable amide/imidic acid tautomeric form (Figure 2). Relative energies at B3LYP/6-311++G** level show that the most stable conformation of tautomer **T1** (II_{T1} amide, NHCH═O) is clearly favored over the most stable tautomer **T2** (IV_{T2} imidic acid, N═CHOH) with an energy difference above 40.0 kJ mol^{-1}; so that, to carry out the subsequent conformational study of our compounds of interest, we only focused on the possible geometries derived from **T1** series.

The combination of the *E*/*Z* imine isomerism (*N*-acylhydrazone) and three rotational axes, $\mathbf{r_1}$ ($C1_{A1}$—$C_{C=O}$), $\mathbf{r_2}$ ($C_{C=O}$—N_{NH}), and $\mathbf{r_3}$ ($C_{N=C}$—$C1_{B1}$), afforded a total of 32 potential geometries corresponding to 16 pairs of conformational enantiomers due to the top/bottom arrangement of the planes defined by the aromatic rings (Figure 3).

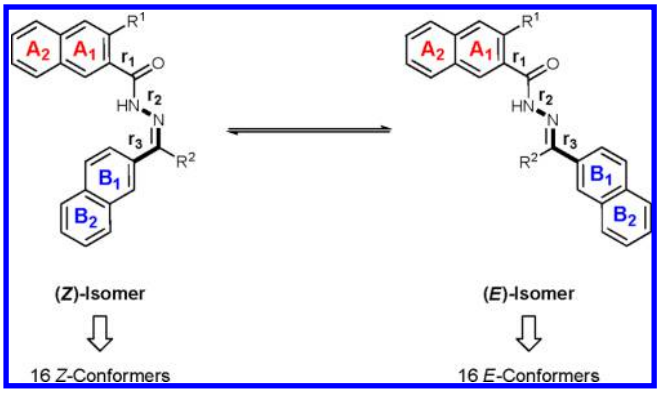

Figure 3. *E*/*Z* isomerism in 3-hydroxy-*N*′-(naphthalen-2-ylmethylene)-2-naphthohydrazide derivatives.

Figures 4 and 5 show the geometries of the structures studied for compounds **1** and **2a**−**c**. In general, we will call the orientation shown in Figure 3 by the **A1A2** rings horizontal (*h*) and that shown by the **B1B2** rings vertical (*v*). With this in mind we consider it useful to make some conformational clarifications before the energy discussion:

- Naphthalene ring **A** presents four possible orientations for each *E*/*Z* isomer as a consequence of the rotation of the $\mathbf{r_1}$ and $\mathbf{r_2}$ axes: $\mathbf{A}_{h1}$ [Z_1, Z_5, E_1, E_5], $\mathbf{A}_{h2}$ [Z_3, Z_7, E_3, E_7], $\mathbf{A}_{v1}$ [Z_2, Z_6, E_2, E_6] and $\mathbf{A}_{v2}$ [Z_4, Z_8, E_4, E_8].
- Naphthalene ring **B** presents two possible orientations for each *E*/*Z* isomer as a consequence of the rotation of

dx.doi.org/10.1021/ci300299n | J. Chem. Inf. Model. 2012, 52, 2387−2397

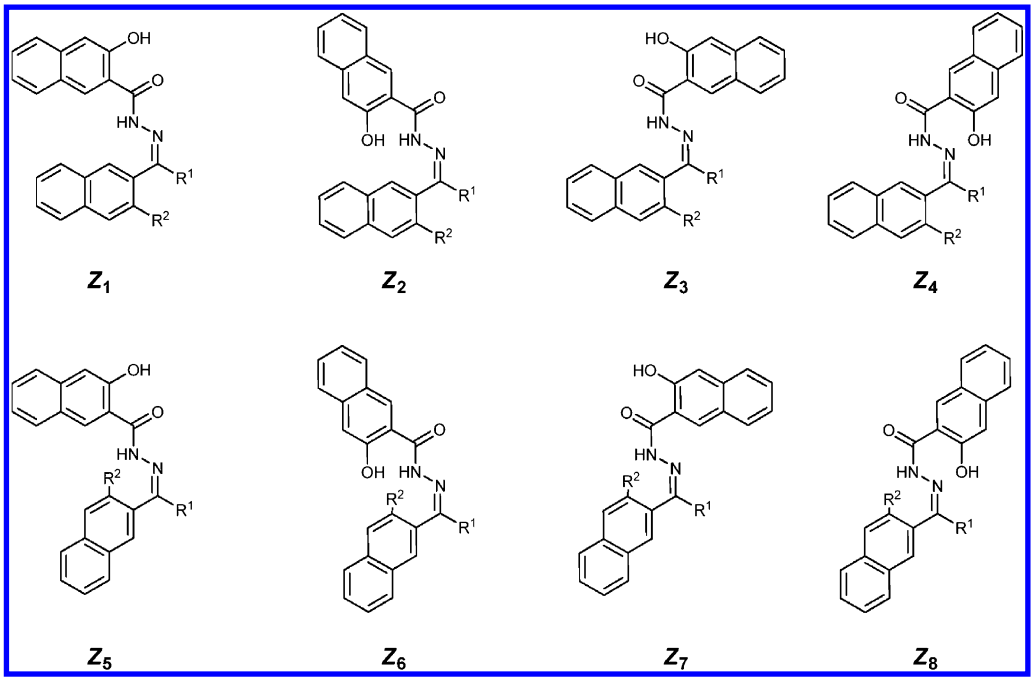

Figure 4. (*Z*)-Conformers of compounds **1** [R^1 = H, R^2 = OH] and **2a–c** [R^1 = H, CH_3 and Ph, respectively, R^2 = H].

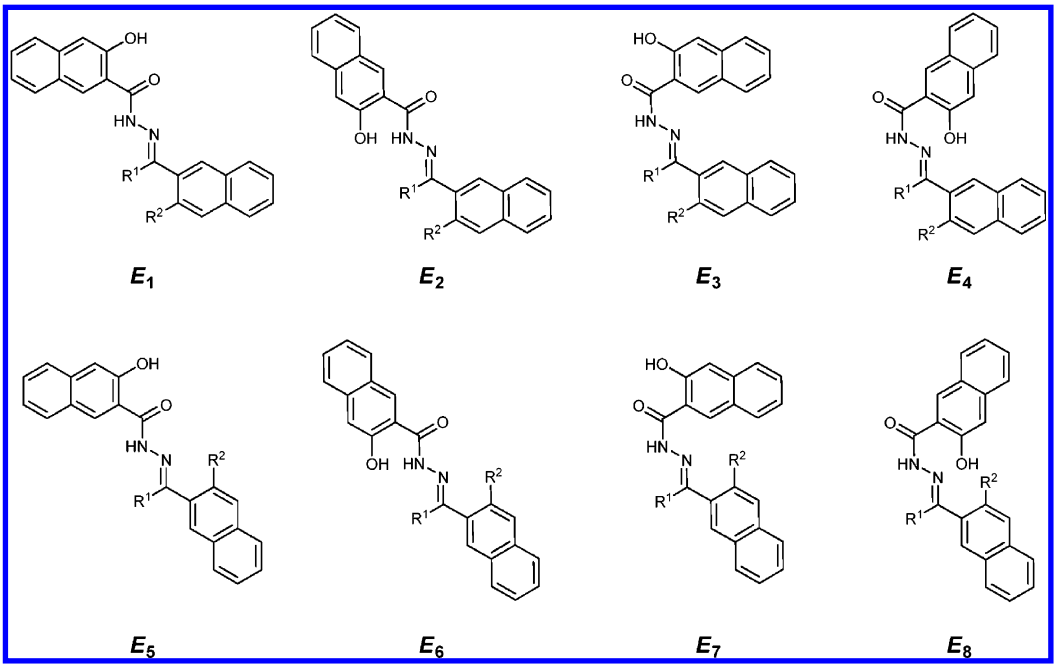

Figure 5. (*E*)-Conformers of compounds **1** [R^1 = H, R^2 = OH] and **2a–c** [R^1 = H, CH_3 and Ph, respectively, R^2 = H].

the $\mathbf{r}_3$ axis: $\mathbf{B}_h$ [Z_1, Z_2, Z_3, Z_4, E_1, E_2, E_3, E_4] and $\mathbf{B}_v$ [Z_5, Z_6, Z_7, Z_8, E_5, E_6, E_7, E_8].

2.2. DFT Energy Analysis. Sixteen minima were optimized for compounds **1** and **2a–c** at the B3LYP/6-311++G** level. As expected, most of the conformers presented a twisted geometry to avoid steric repulsions between the naphthalene rings and/or the linker. Conformers E_2 and E_6 were an exception, showing an almost planar arrangement of the rings due to the more favorable anti orientation of the aromatic groups and a stabilizing orientation of the hydroxyl groups.

The relative free energies of the minima are gathered in Table 2. The gas phase values show that in series **1** [R^1 = H, R^2 = OH], the absolute minimum corresponds to the conformer E_5, with a difference of 37.4 kJ mol^{-1} compared to the most favorable *Z* conformation (Z_3). In series **2a** [R^1 = H, R^2 = H], this corresponds to the conformer E_7 with a lower difference of 19.3 kJ mol^{-1} (Z_3). Therefore, in both cases the *E*/*Z* energy gap suggests an almost quantitative shift of the equilibrium to the *E* isomer which should appear a priori as the most abundant product in experimental conditions. The possibility of establishing a highly stabilized intramolecular hydrogen bond interaction (IMHB) between the OH substituent of the naphthalene ring **B1** and the imine nitrogen lone pair ($\mathbf{OH_{B1}}\cdots\mathbf{N_{N=C}}$) explains the increase in the energy *E*/*Z* ratio of compound **1** (E_5) with regard to **2a** (E_7) (Figure 6).

dx.doi.org/10.1021/ci300299n | *J. Chem. Inf. Model.* 2012, 52, 2387–2397

Table 2. Relative Free Energies (kJ mol^{-1}) of All Optimized Geometries at the B3LYP/6-311++G Level in Gas Phase and PCM (Water) Continuum Model**

conformer	G_{rel} (**1**) gas	G_{rel} (**1**) water	G_{rel} (**2a**) gas	G_{rel} (**2a**) water	G_{rel} (**2b**) gas	G_{rel} (**2b**) water	G_{rel} (**2c**) gas	G_{rel} (**2c**) water
Z_1	42.2	37.2	24.1	24.8	6.4	3.5	3.4	3.0
Z_2	61.5	48.8	40.0	33.8	25.8	14.4	22.4	14.0
Z_3	37.4	44.5	19.3	30.4	4.6	12.3	4.0	11.9
Z_4	54.1	55.1	34.5	38.8	20.1	19.7	20.6	25.7
Z_5	44.2	37.6	23.8	24.1	7.0	4.7	3.9[a]	3.0[a]
Z_6	65.9	51.1	61.4	52.9	26.6	15.0	22.4[a]	14.0[a]
Z_7	40.0	46.2	19.8	31.8	4.5	12.3	4.0[a]	11.9[a]
Z_8	54.0	52.6	34.9	38.1	20.6	20.4	20.6[a]	25.7[a]
E_1	22.5	18.8	5.8	3.8	6.6	0.3	4.4	6.0
E_2	38.6	23.3	25.0	10.6	22.8	10.3	23.7	15.4
E_3	20.4	27.0	3.0	11.0	2.2	7.4	4.9	12.9
E_4	36.2	37.4	19.7	21.5	17.0	15.6	21.2	22.2
E_5	**0.0**	**0.0**	2.4	**0.0**	2.8	**0.0**	**0.0**	**0.0**
E_6	14.9	12.1	22.0	15.2	18.8	5.7	19.9	9.3
E_7	6.2	14.0	**0.0**	7.6	**0.0**	5.5	1.2	9.6
E_8	29.6	29.4	16.8	18.7	15.2	12.7	17.9	25.3

[a]The geometries Z_5, Z_6, Z_7, and Z_8 evolve spontaneously to the same minima Z_1, Z_2, Z_3, and Z_4, respectively.

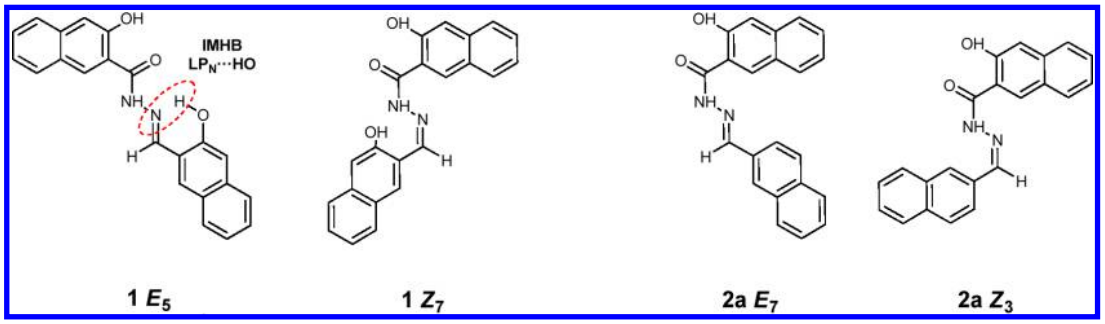

Figure 6. Most stable *E* and *Z* conformers for compounds **1** and **2a**, respectively.

Focusing on series **2**, the increase in the size of the R^1 substituent produces a reduction in the *E*/*Z* energy gap from 19.3 kJ mol^{-1} in **2a** [R^1 = H, R^2 = H] to 4.6 kJ mol^{-1} in **2b** [R^1 = CH_3, R^2 = H]. In series **2c** [R^1 = Ph, R^2 = H], a near parity in the energy difference—E_5 is the absolute minimum, only 3.4 kJ mol^{-1} below the best *Z* conformation (Z_1)—is observed. The small energy difference for **2c** suggests that the distribution of *E* and *Z* isomers will be fairly similar, a result that could be reflected experimentally as an isomeric mixture. It can be inferred that in series **2** the steric hindrance determines the *E*/*Z* distribution ratio.

A major consideration for us is to simulate the compounds in condition of biological relevance. Accordingly, all the conformers have also been calculated in water solvent phase using the pcm continuum model. As would be expected, slight differences are presented in the relative energies with regard to the gas phase results. However, the general trend confirms the prevalence of the *E* isomer for compounds **1** and **2a**, even in aqueous conditions. Moreover, the potential *E*/*Z* isomeric mixture due to the narrow energy range between isomers for compound **2c** is similarly observed in water phase calculations.

As described for naphthalene **B**, in compound **1**, the relative orientation of the hydroxyl group of ring **A** plays a major role in the stabilization of the conformers due to the possibility of establishing up to three different types of IMHB interactions (Figure 7): (1) $\mathbf{OH_{A1}}$···$\mathbf{O_{C=O}}$ [Z_1, Z_3, Z_5, Z_7, E_1, E_3, E_5, E_7]; (2) **NH**···$\mathbf{OH_{A1}}$ [Z_2, Z_6, E_2, E_6], and (3) $\mathbf{OH_{A1}}$···$\mathbf{N_{N=C}}$ [Z_4, Z_8, E_4, E_8]. Clustering those conformers that share the same

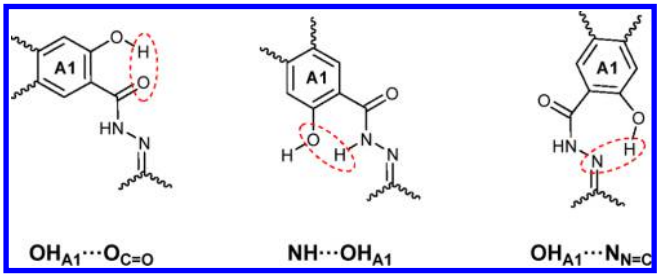

Figure 7. IMHB interactions of naphthalene ring A.

arrangement of naphthalene ring **B**, we observe systematically that the relative free energies in gas phase follow the trend $Z/E_3 < Z/E_1 < Z/E_4 < Z/E_2$ and $Z/E_7 < Z/E_5 < Z/E_8 < Z/E_6$ for the $\mathbf{B_h}$ and $\mathbf{B_v}$ conformers, respectively. An exception are the E_5–E_8 conformers of compound **1** where the presence of the hydroxyl group in **B1** distorts this general trend. This pattern is not observed in water phase due to the decrease of the hydrogen bonding stabilizing contribution to the energy due to solvation effects. The main conclusion is that the degree of stabilization induced by the HB interaction type $\mathbf{OH_{A1}}$···$\mathbf{O_{C=O}}$ is significantly higher than that induced by $\mathbf{OH_{A1}}$···$\mathbf{N_{N=C}}$ or **NH**···$\mathbf{OH_{A1}}$, which is in a narrow energy range playing a significant role in the observed rearrangement determined by the NMR structural study.

Although E_1 and E_5 conformers suffer an energy penalty resulting from repulsion between the $H1_{A1}$ and NH hydrogen

dx.doi.org/10.1021/ci300299n | J. Chem. Inf. Model. 2012, 52, 2387−2397

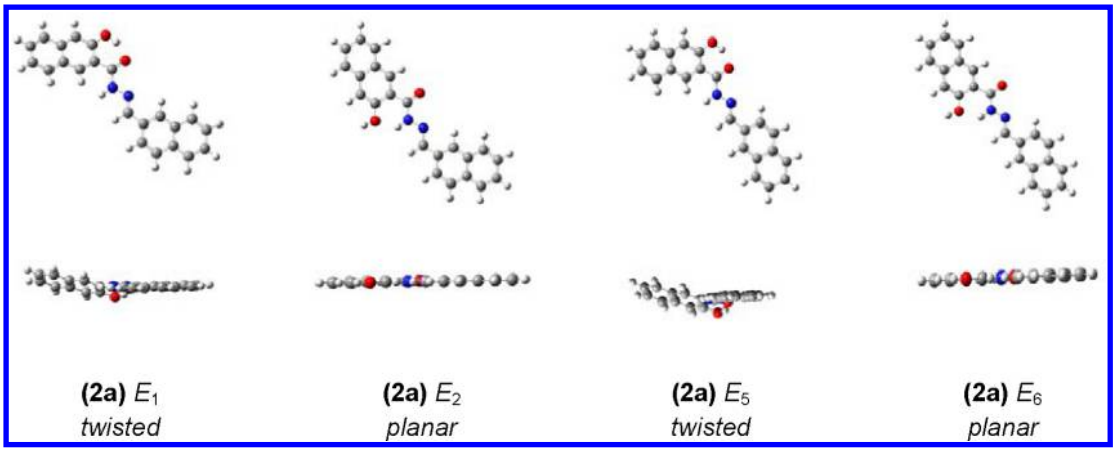

Figure 8. $OH\cdots O_{C=O}$ (E_1 and E_5) vs $NH\cdots O_{OH}$ (E_2 and E_6) stabilization.

Scheme 2. General Synthetic Pathway of 3-Hydroxy-*N*′-(naphthalen-2-ylmethylene)-2-aromatic Hydrazides Derivatives (*R* = H, CH_3, Ph)

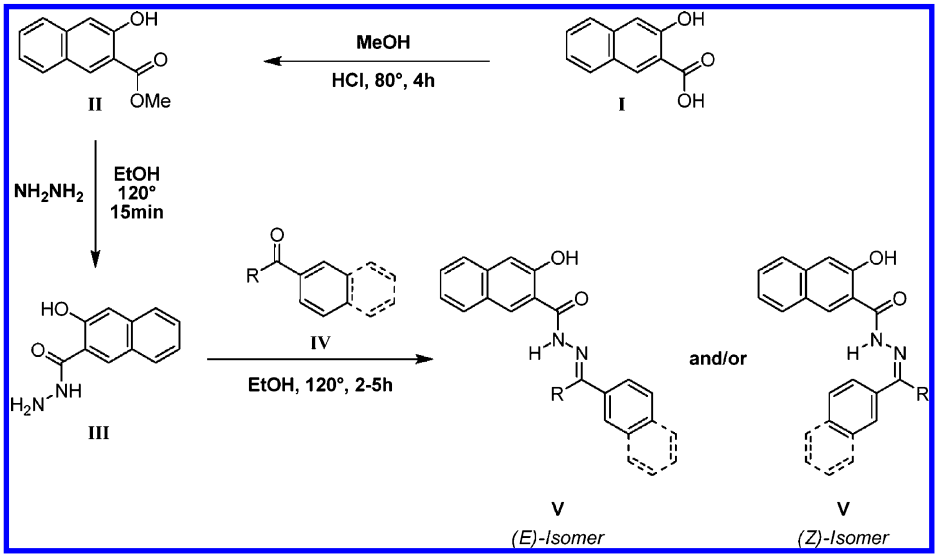

atoms which breaks the planarity of the system, they show in all cases a substantial increase in stability when compared to their respective planar rotamers E_2 and E_6, emphasizing the prevalence of the $OH_{A1}\cdots O_{C=O}$ stabilization (Figure 8) both in gas and water phase.

2.3. Synthesis of 3-Hydroxy-*N*′-((naphthalen-2-yl)-methylene)naphthalene-2-carbohydrazide Derivatives. A series of 3-hydroxy-*N*′-((naphthalen-2-yl)methylene)-naphthalene-2-carbohydrazides (**2a**−**c**) analogs and the closely related *N*′-benzylidene-3-hydroxy-2-naphthohydrazide (**3**) were synthesized following a standard synthetic route (Scheme 2). Starting from the commercially available 3-hydroxy-2-naphthoic acid (**I**), an esterification was performed in the presence of hydrochloric acid to afford the corresponding methyl 3-hydroxynaphthalene-2-carboxylate intermediate (**II**). Treatment of **II** with hydrazine hydrate afforded the hydrazide **III**. Condensation of **III** with the appropriate aldehyde or ketone (**IV**) afforded the products (**V**) in good yields. Systems **2a**, **2b**, and **3** were isolated as a single isomer, and subsequently characterized by ^{1}H NMR as the *E* isomer. Compound **2c**, however, resulted as an inseparable mixture of *E*/*Z* isomers (see structure **V**) consistent with our theoretical predictions.

2.4. NMR Characterization. A combination of different NMR spectroscopic methodologies has been employed for the unequivocal characterization of the compounds studied in this work. Figure 9 shows the ^{1}H NMR spectroscopic signals within the range of 7.0−12.4 ppm corresponding to the series **2a**−**c**. This region includes all the aromatic hydrogen atoms as well as NH/OH hydrogen atoms present in these compounds. Two important conclusions are evident, corroborating our theoretical predictions:

1. The spectra of compounds **2a** [R^1 = H] and **2b** [R^1 = CH_3] correspond to an almost quantitative single isomer (a minimal trace of the second isomer is observed); conversely, compound **2c** [R^1 = Ph] presents duplicated signals for all protons—indicating, as predicted, a mixture of isomers.
2. OH hydrogen atoms are strongly displaced downfield with chemical shift values above 10.0 ppm clearly indicating their participation in an intramolecular hydrogen bond with the lone pairs of the carbonyl oxygen atom.

Figure 10 illustrates the most significant intramolecular interactions which were probed by NMR and employed for the correct assignment of the experimentally obtained isomers for

dx.doi.org/10.1021/ci300299n | J. Chem. Inf. Model. 2012, 52, 2387−2397

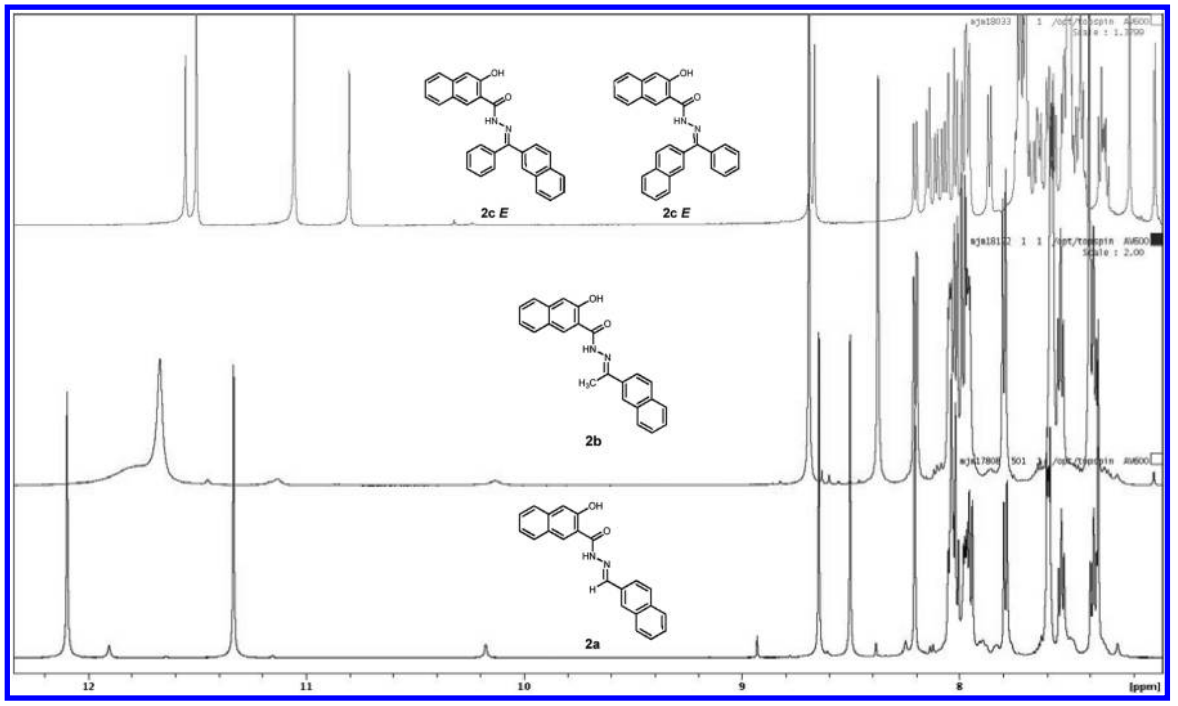

Figure 9. ^{1}H NMR spectra of compounds **2a**–**c**.

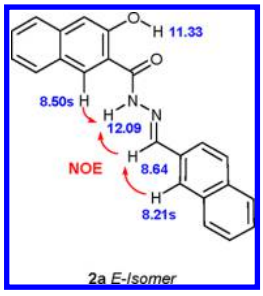

Figure 10. Relevant spectroscopic data used for NMR structure elucidation (**2a**).

compound **2a**. Irradiation of the hydrogen corresponding to the R^2 group H (8.64 ppm) in NOE experiments resulted in the perturbation of the NH signal at 12.09, demonstrating the *E* character of the isolated isomer (a hypothetical *Z* isomer could not show this NOE interaction due to the greater distance between the involved groups). A similar result was obtained in the NOE analysis of compound **2b** when the R^2 signal of CH_3 (2.52 ppm) was irradiated.

Moreover, additional NOE experiments confirmed that $R^1 \gg$ H1′ singlet [**B1** ring] and NH ≫ H1 singlet [**A1** ring] interactions, in addition to the observed $\mathbf{OH_{A1}}\cdots\mathbf{O_{C=O}}$ IMHB, all of which confirm the most probable/favorable conformation of the studied compounds under the experimental conditions.

2.5. X-ray Analysis. Confirmation of the NMR experimental data and computational predictions was achieved with the X-ray crystal analysis. Slow recrystallization of compound **2a** from methanol provided the crystal structure of (*E*)-3-hydroxy-*N*′-((naphthalen-2-yl)methylene)-naphthalene-2-carbohydrazide as an isolated *E* isomer (Figure 11).

A review of available data identified eight other crystal structures of very similar compounds deposited within the Cambridge Crystallographic Database (CSD).[28] As shown (Figure 12), all of them present an *E* geometry, consistent with our results.

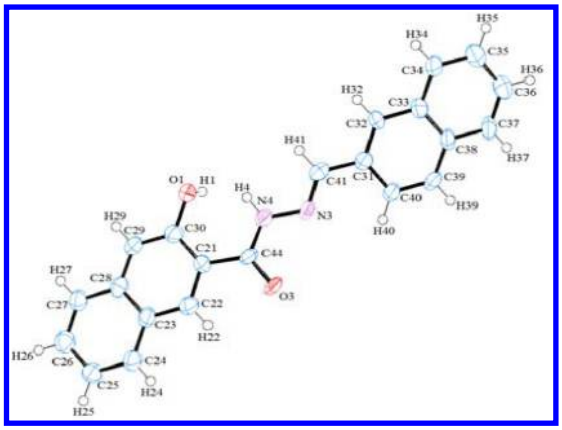

Figure 11. Crystal structure of (*E*)-3-hydroxy-*N*′-((naphthalen-2-yl)methylene)naphthalene-2-carbohydrazide (**2a**) obtained in this work (Ortep representation).

With reference to the specific orientation of the naphthalene ring **A**, both in the newly obtained structure (**2a**) and in that previously reported in the literature, with the exception of the structures RUJJEM and CICNUY, the preferential conformation observed corresponds to the E_2/E_6 conformers, observed in almost all cases (See Figure 5 and Table 2 for comparison), and not to the expected absolute minimum E_7. This discrepancy may be explained by the fact that crystal packing forces tend to favor the most planar geometry, and on this basis, E_2/E_6 would be the preferential conformation as discussed above. However, we can not assume that this constitutes a complete explanation because the observed arrangement of the compounds analyzed does not follow a standard stacking pattern (See packing geometry of referenced structures). Another interesting observation is that the substitution of the hydroxyl group (HUGPOP) by a methoxy one (RUJKOX) induces the rotation of the phenyl ring in order to favor the most stable geometry based on the hydrogen

dx.doi.org/10.1021/ci300299n | J. Chem. Inf. Model. 2012, 52, 2387–2397

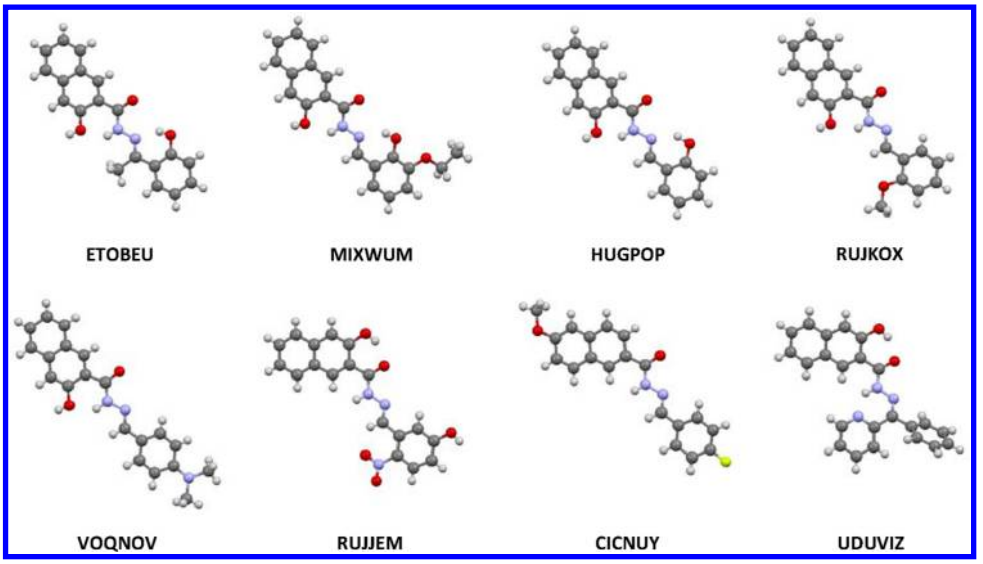

Figure 12. Crystallographic structures of related compounds found in the CSD (compound labels correspond to the CSD codes).

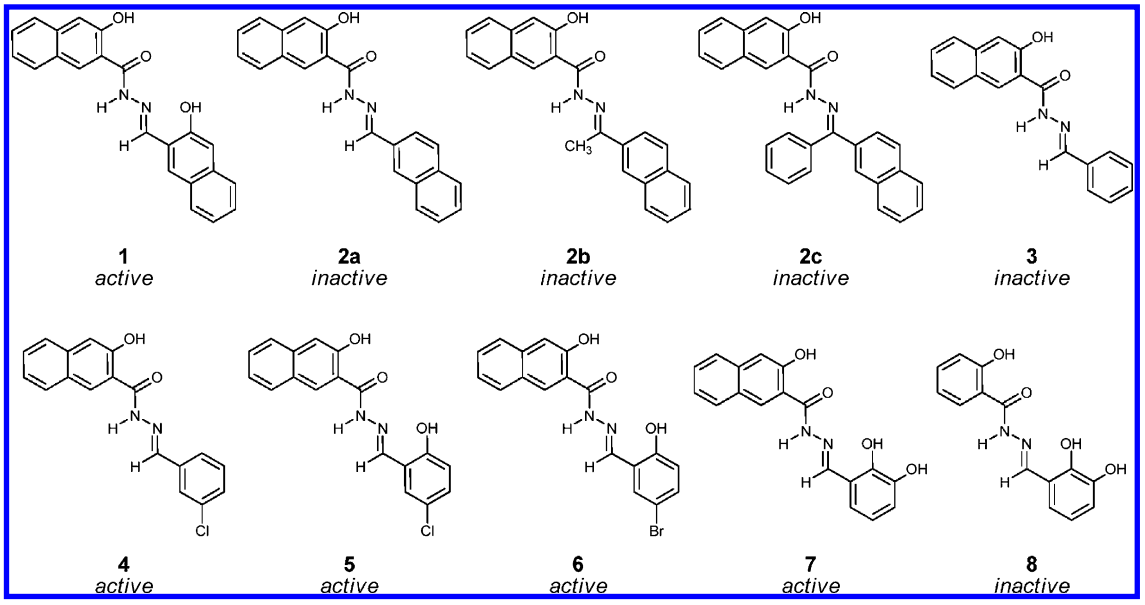

Figure 13. Series of diarylhydrazides assayed on AR TR-FRET.

bonding network, so it is possible to achieve some conformational control of the rotational state, depending on the properties of the substituent, which is very interesting from a pharmacological point of view.

On the basis of our results, and the data found in the literature, we can conclude the following for this class of compounds:

1. The *E*/*Z* isomeric equilibrium is strongly governed by the ratio of the size (steric hindrance) of the substituents on the imine group.
2. Free rotation around the $\mathbf{r}_1$ and $\mathbf{r}_3$ axes in solution favors a higher representation of the thermodynamically most stable conformer as determined by the balance between the stabilizing (IMHB)/repulsive effect of the substituents.
3. The available crystallographic data suggests that the preferential conformation in the solid state is strongly determined by packing forces, but all the reported structures are found as *E* isomers, which is consistent with our theoretical studies.

2.6. Biological Study. We present the biological evaluation of ten different diarylhydrazide compounds (Figure 13), including those conformationally studied in this work (**1**−**2**), for their ability to displace AR:coactivator interaction using TR-FRET techniques.

The TR-FRET technique measures the recruitment of a fluorescent (Fl) labeled coactivator (of the AR specific FxxLF type: acceptor) to a Terbium (Tb) labeled GST tagged AR-LBD (donor). The technique is dependent on the distance between the donor/acceptor pair.[29] In the case of an agonist bound LBD, the Fl labeled coactivator is associated with LBD, so when Tb is excited at 340 nm, energy is transferred to Fl resulting in an increase in TR-FRET signal. In the presence of an antagonist, the Fl coactivator is not bound to the LBD; therefore, energy cannot be successfully transferred from Tb to Fl resulting in a decrease of the TR-FRET signal. Data is presented as a percentage maximum of activity as described

dx.doi.org/10.1021/ci300299n | J. Chem. Inf. Model. 2012, 52, 2387−2397

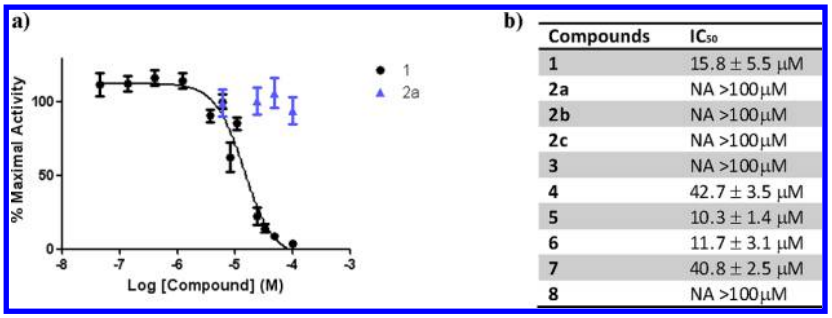

Compounds	IC_{50}
1	15.8 ± 5.5 μM
2a	NA >100 μM
2b	NA >100 μM
2c	NA >100 μM
3	NA >100 μM
4	42.7 ± 3.5 μM
5	10.3 ± 1.4 μM
6	11.7 ± 3.1 μM
7	40.8 ± 2.5 μM
8	NA >100 μM

Figure 14. (a) Dose response curve for (**1**) and its closest analog (**2a**). Compounds were tested using a maximum concentration of 100 μM in the presence of a concentration of DHT (endogenous agonist) equal to its EC_{80} concentration (see the Experimental Section). Data points are presented as standard error of mean (SEM) of at least two independent experiments in triplicate. Data was fitted using the dose−response curve (variable slope). (b) Diarylhydrazides activity toward AR-LBD. Values are presented as IC_{50} ± SEM of at least two independent experiments where each well was included as triplicate.

previously,[30] and the binding data of the tested compounds is presented in Figure 14.

Qualitative SAR Analysis. Derived from our biological evaluation of targeted modifications of the diarylhydrazide scaffold, we can determine some initial qualitative SAR conclusions:

1. The OH group on naphthalene ring B seems important for activity when comparing **1**/**2a**, **7**/**3**, and **5**/**4** pairs of analogs. If not present, it abolishes (**2a** and **3**) or diminishes (**4**) the activity.
2. Naphthalene ring **A2** seems to be required when comparing **7**/**8** pair since the substitution of naphthalene by a benzene ring abolishes the activity (**8**).
3. Compounds **1**, **5**, and **6** are equipotent, demonstrating that the presence of naphthalene ring B2 (**1**) or a hydrophobic group like chlorine (**5**) or bromine (**6**) increase the activity on AR.

3. CONCLUSIONS

The preferred molecular conformations for four 3-hydroxy-*N*′-((naphthalen-2-yl)methylene)naphthalene-2-carbohydrazides have been modeled using DFT theoretical calculations and experimentally determined through solution NMR and crystallographic diffraction analysis. Their isomerism and conformational space, including that of some simpler models, have been fully determined. The energy ranges between isomers depend on a number of factors, the most important of which are the formation of intramolecular hydrogen bonds and steric effects. Under experimental conditions, we have demonstrated that the *E*-isomer is formed under the described synthetic conditions for this family of compounds. The *Z*-isomer is formed when the steric hindrance of the second imine substituent is sufficiently high, in this case as an equal mixture with the corresponding *E*-isomer. This is in full agreement with the theoretical predictions.

Additionally, the biological activity of ten diarylhydrazides analogs as non-ligand binding pocket antagonists of the androgen receptor, including those synthesized in this work, has been determined using TR-FRET. This preliminary SAR evaluation highlights the importance of naphthalene ring placement for compound binding and should be considered when advancing future series of non-LBP AR binding analogs.

It is important to note that these diarylhydrazides have been characterized as non-LBP AR antagonists—they do not bind in an enclosed pocket. The proposed mechanism of action is a functional disruption of AR interaction with coactivators on the surface of AR LBD. With this unambiguous determination of molecular conformational preference, and ahead of resolution of any X-ray cocrystal structure of the protein:ligand complex for these compounds, this study now affords a significant starting point for structure-based expansion of this molecular series.

4. EXPERIMENTAL SECTION

4.1. General Experimental Data.[31] All commercially available reagents were purchased and used without further purification unless otherwise indicated. Dichloromethane was dried by distillation from calcium hydride prior to use. IR spectra were recorded as thin films on NaCl plates or as KBr discs on a 100 FT-IR spectrometer. ^{1}H and ^{13}C NMR spectra were obtained at 20 °C, 400.13 MHz for ^{1}H spectra, 100.61 MHz for ^{13}C spectra, in $(CD_3)_2SO$ (internal standard tetramethylsilane). High resolution accurate mass determinations for all final target compounds were obtained and recorded by electrospray ionization mass spectrometry (ESI-MS), which was performed in the positive ion mode on a liquid chromatography time-of-flight mass spectrometer. Thin layer chromatography was performed using Silica gel 60 TLC aluminum sheets with fluorescent indicator visualizing with UV light at 254 nm. Flash chromatography was carried out using standard silica gel 60 (230−400 mesh).

4.2. General Procedure for the Synthesis of 3-Hydroxy-*N*′-(naphthalen-2-ylmethylene)-2-naphthohydrazides (Scheme 2). *4.2.1. Methyl 3-Hydroxynaphthalene-2-carboxylate (II).* 3-Hydroxy-2-naphthoic acid (3.76 g, 20 mmol) was added to a solution of MeOH (20 mL) and HCl 37% (20 mL). The reaction mixture was heated at 90 °C and the esterification was monitored on TLC until complete consumption of the starting material was observed. Solvent was then removed in vacuo, and the reaction mixture was diluted with CH_2Cl_2 (30 mL) and washed with H_2O, CH_2Cl_2 (2 × 30 mL), and saturated aqueous $NaHCO_3$. The aqueous phase was extracted and the combined organic layers were dried over anhydrous Na_2SO_4, filtered, and concentrated in vacuo to give the crude product. The crude mixture was purified by flash column chromatography over silica gel (eluent 9:1, CH_2Cl_2/MeOH) to afford II (Scheme 2) as a colorless solid (2.17 g, 65%, lit. MP: 73−75 °C).[32]

4.2.2. 3-Hydroxynaphthalene-2-carbohydrazide (III). To a solution of **II** (2.02 g, 10 mmol) in EtOH (10 mL), hydrazine hydrate was added (1.245 mL, 40 mmol) and the reaction mixture was heated to 120 °C until complete precipitation of

hydrazide occurred (15 min). Completion of the reaction was confirmed by TLC. The reaction mixture was allowed to cool to 20 °C, filtered and washed with hexane to give **III** as a beige powder (2.01 g, 99%, lit. MP: 205−208 °C).[33]

*4.2.3. (E)-3-Hydroxy-N′-((naphthalen-2-yl)methylene)-naphthalene-2-carbohydrazide (**2a**).* To a solution of **III** (1.534 g, 7.5 mmol) in EtOH (20 mL), 2-naphthaldehyde was added (1.1713 g, 7.5 mmol), the reaction was heated to 120 °C and monitored by TLC until complete consumption of the starting material was observed (6 h). The reaction mixture was allowed to cool to 20 °C, filtered, and washed with hexane to give a pale yellow powder identified as **2a** (2.2 g, 86%, MP: 276−280 °C). IR (KBr) υ_{max}: 3439.93 (OH stretch), 3054.38 (NH stretch), 1625.69 (C═O stretch) cm^{-1}. ^1H NMR (600 MHz, DMSO-d_6): δ 12.09 (s, *NH*), 11.33 (s, *OH*), 8.64 (s, 1H, H_{CN}), 8.50 (s, 1H, H_1), 8.21 (s, 1H, $H_{1'}$), 8.04 (d, 1H, $H_{3'}$), 8.03 (d, 1H, $H_{8'}$), 8.02 (d, 1H, $H_{4'}$), 7.98 (d, 1H, $H_{5'}$), 7.95 (d, J = 8.3 Hz, 1H, H_8), 7.79 (d, J = 8.2 Hz, 1H, H_5), 7.59 (dd, 1H, $H_{6'}$), 7.58 (dd, 1H, $H_{7'}$), 7.53 (dd, J_1 = 8.2 Hz, J_2 = 7.5 Hz, 1H, H_6), 7.39 (dd, J_1 = 8.3 Hz, J_2 = 7.5 Hz, 1H, H_7), 7.36 (s, 1H, H_4) ppm. ^{13}C NMR (600 MHz, DMSO-d_6): δ 163.8 (q, C_{CO}), 154.1 (q, C_3), 148.4 (q, C_{CN}), 135.8 (q Ar, C_{10}), 133.8 (q Ar, $C_{10'}$), 131.9 (q Ar, $C_{2'}$), 130.2 (CH Ar, C_1), 129.0 (CH Ar, $C_{1'}$), 128.6 (CH Ar, C_8), 128.5 (CH Ar, $C_{4'}$), 128.4 (CH Ar, $C_{8'}$), 128.2 (CH Ar, C_6), 127.8 (CH Ar, $C_{5'}$), 127.2 (CH Ar, $C_{6'}$), 126.8 (q Ar, C_9), 126.8 (q Ar, $C_{9'}$), 126.8 (CH Ar, $C_{7'}$), 125.8 (CH Ar, C_5), 123.8 (CH Ar, C_7), 122.7 (CH Ar, $C_{3'}$), 120.4 (q Ar, C_2), 110.5 (CH Ar, C_4) ppm. HRMS: $C_{22}H_{17}N_2O_2$ $[M + H]^+$ requires (m/e) 341.1290, found 341.1296

*4.2.4. (E)-3-Hydroxy-N′-(1-(naphthalen-2-yl)ethylidene)-naphthalene-2-carbohydrazide (**2b**).* To a solution of **III** (1.01 g, 5 mmol) in EtOH (20 mL), 2-acetonaphthone was added (850 mg, 5 mmol), the reaction was heated to 120 °C and monitored by TLC until complete consumption of the starting material was observed (3 h). The reaction mixture was allowed to cool to 20 °C, filtered, and washed with hexane to give a pale yellow powder identified as **2b** (1.48 g, 84%, MP: 275−280 °C). IR (KBr) υ_{max}: 3369.86 (OH stretch), 3052.55 (NH stretch), 1627.45 (C═O stretch) cm^{-1}. ^1H NMR (600 MHz, DMSO-d_6): δ 11.69 (s, *OH*), 11.67 (s, *NH*), 8.67 (s, 1H, H_1), 8.37 (s, 1H, $H_{1'}$), 8.20 (d, J = 8.52 Hz, 1H, $H_{3'}$), 8.05 (d, 1H, $H_{8'}$), 8.02 (d, J = 8.0 Hz, 1H, H_8), 7.98 (d, 1H, $H_{4'}$), 7.97 (d, 1H, $H_{5'}$), 7.80 (d, J = 8.0 Hz, 1H, H_5), 7.58 (dd, 1H, $H_{6'}$), 7.57 (dd, 1H, $H_{7'}$), 7.54 (dd, J_1 = 8.0 Hz, J_2 = 7.3 Hz, 1H, H_6), 7.40 (s, 1H, H_4), 7.39 (dd, J_1 = 8.0 Hz, J_2 = 7.3 Hz, 1H, H_7), 2.52 (s, 3H, H_{Me}) ppm. ^{13}C NMR (600 MHz, DMSO-d_6): δ 161.6 (q, C_{CO}), 152.8 (q, C_3), 152.0 (q, C_{CN}), 135.8 (q Ar, C_{10}), 135.3 (q Ar, $C_{2'}$), 133.4 (q Ar, $C_{10'}$), 132.8 (q Ar, $C_{9'}$), 132.3 (CH Ar, C_1), 128.9 (CH Ar, C_8), 128.6 (CH Ar, $C_{8'}$), 128.3 (CH Ar, C_6), 127.8 (CH Ar, $C_{4'}$), 127.5 (CH Ar, $C_{5'}$), 127.2(q Ar, C_9), 126.9 (CH Ar, $C_{6'}$), 126.6 (CH Ar, $C_{1'}$), 126.5 (CH Ar, $C_{7'}$), 125.7 (CH Ar, C_5), 123.9 (CH Ar, C_7), 123.7 (CH Ar, $C_{3'}$), 120.8 (q Ar, C_2), 110.7 (CH Ar, C_4), 13.7 (CH_3) ppm. HRMS: $C_{23}H_{19}N_2O_2$ $[M + H]^+$ requires (m/e) 355.1447, found 355.1459.

*4.2.5. (E/Z)-3-Hydroxy-N′-((naphthalen-2-yl)(phenyl)-methylene)naphthalene-2-carbohydrazide (**2c**).* To a solution of **III** (404 mg, 2 mmol) in EtOH (10 mL), 2-benzoylnaphthalene was added (464 mg, 2 mmol), the reaction was heated to 120 °C and monitored by TLC until complete consumption of the starting material was observed (5 h). The reaction mixture was purified by flash column chromatography over silica gel (eluent 9:1, CH_2Cl_2/MeOH) to give a pale brown resin identified as a mixture of E/Z isomers **2c** (50 mg, 5%, MP: 295−298 °C). IR (KBr) υ_{max}: 3482.27 (OH stretch), 3149.78 (NH stretch), 1620.74 (C═O stretch) cm^{-1}. ^1H NMR (600 MHz, DMSO-d6): δ 11.56 (s, *NH*), 11.51 (s, *NH*), 11.06 (s, *OH*), 10.81 (s, *OH*), 8.68 (s, 1H, H_2), 8.66 (s, 1H, H_1), 7.71 (t, 1H, H_{21}), 7.44 (m, 1H, H_{32}), 7.73 (t, 1H, H_{20}), 8.20 (d, 1H, H_5), 7.97 (d, 1H, H_{18}), 7.96 (d, 1H, H_{19}), 7.86 (d, 1H, H_{22}), 8.07 (d, 1H, H_{26}), 7.43 (m, 1H, H_{27}), 7.49 (m, 1H, H_{30}), 7.46 (t, 1H, H_{31}), 7.49 (m, 1H, H_{29}), 7.69 (m, 1H, H_{28}), 8.01 (d, 1H, H_{25}), 8.10 (d, 1H, H_{24}), 8.05 (s, 1H, H_{23}), 7.96 (d, 1H, H_{17}), 7.59 (d, 1H, H_{15}), 7.69 (d, 1H, H_{16}), 7.57 (t, 1H, H_{14}), 7.64 (t, 1H, H_{13}), 7.52 (s, 1H, H_{12}), 7.69 (m, 1H, H_{10}), 7.63 (t, 1H, H_9), 7.51 (m, 1H, H_{11}), 7.35 (d, 1H, H_8), δ 7.33 (t, 1H, H_7), δ 8.14 (d, 1H, H_6), δ 7.21 (s, 1H, H_4) δ 7.10 (s, 1H, H_3) ppm. ^{13}C NMR (600 MHz, DMSO-d_6): δ 128.53 (CH Ar, C_{52}), 129.80 (CH Ar, C_{51}), 120.20 (CH Ar, C_{50}), 110.50 (CH Ar, C_{49}), 110.54 (CH Ar, C_{48}), 120.19 (CH Ar, C_{47}), 123.86 (CH Ar, C_{46}), 123.93 (CH Ar, C_{45}), 123.95 (CH Ar, C_{44}), 125.32 (CH Ar, C_{43}), 125.63 (CH Ar, C_{42}), 125.67 (CH Ar, C_{41}), 126.75 (CH Ar, C_{40}), 126.96 (CH Ar, C_{39}), 127.17 (CH Ar, C_{38}), 127.20 (CH Ar, C_{37}), 127.23 (CH Ar, C_{36}), 127.37 (CH Ar, C_{35}), 127.58 (CH Ar, C_{34}), 127.63 (CH Ar, C_{33}), 128.07 (CH Ar, C_{32}), 128.09 (CH Ar, C_{31}), 128.14 (CH Ar, C_{30}), 128.21 (CH Ar, C_{29}), 128.29 (CH Ar, C_{28}), 128.39 (CH Ar, C_{27}), 128.44 (CH Ar, C_{26}), 128.52 (CH Ar, C_{25}), 128.58 (CH Ar, C_{24}), 129.02 (CH Ar, C_{23}), 129.06 (CH Ar, C_{22}), 129.51 (CH Ar, C_{21}), 129.82 (CH Ar, C_{20}), 130.04 (CH Ar, C_{19}), 130.18 (CH Ar, C_{18}), 132.51 (CH Ar, C_{17}), 132.61 (CH Ar, C_{16}), 132.97 (CH Ar, C_{15}), 133.03 (CH Ar, C_{14}), 133.06 (CH Ar, C_{13}), 133.22 (CH Ar, C_{12}), 133.50 (CH Ar, C_{11}), 134.83 (CH Ar, C_{10}), 135.78 (CH Ar, C_9), 135.85 (CH Ar, C_8), 137.38 (CH Ar, C_7), 152.19 (CH Ar, C_6), 152.25 (CH Ar, C_5), 153.73 (CH Ar, C_4), 153.81 (CH Ar, C_3), 160.97 (CH Ar, C_2), 161.12 (CH Ar, C_1). HRMS: $C_{28}H_{20}N_2NaO_2$ $[M + Na]^+$ requires (m/e) 439.14225, found 439.141.

*4.2.6. (E)-N′-Benzylidene-3-hydroxynaphthalene-2-carbohydrazide (**3**).* To a solution of **III** (1.01 g, 5 mmol) in EtOH (20 mL), benzaldehyde was added (0.507 mL, 5 mmol); the reaction was heated to 120 °C and monitored by TLC until complete consumption of the starting material was observed (2 h). The reaction mixture was allowed to cool to 20 °C, filtered, and washed with hexane to give a pale brown powder identified as **3** (1.24 g, 85%, MP: 227−230 °C, lit. MP: 224−225 °C).[34] IR (KBr) υ_{max}: 3242.11 (OH stretch), 3047.11 (NH stretch), 1625.80 (C═O stretch) cm^{-1}. ^1H NMR (600 MHz, DMSO-d_6): δ 11.99 (s, *OH*), 11.30 (s, *NH*), 8.48 (s, 1H, H_{CN}), 8.47 (s, 1H, H_1), 7.93 (d, J = 8.2 Hz, 1H, H_8), 7.79 (d, J = 7.2 Hz, 1H, $H_{2'}$), 7.78 (d, J = 7.2 Hz, 1H, H_5), 7.53 (dd, J_1 = 7.3 Hz, J_2 = 7.3 Hz, 1H, H_6), 7.50 (dd, J = 7.52 Hz, 1H, $H_{3'}$), 7.49 (ddd, $H_{4'}$), 7.38 (dd, J_1 = 8.2 Hz, J_2 = 7.3 Hz, 1H, H_7), 7.34 (s, 1H, H_4) ppm. ^{13}C NMR (600 MHz, DMSO-d_6): δ 163.8 (q, C_{CO}), 154.1 (q, C_3), 148.5 (q, C_{CN}), 135.8 (q Ar, C_{10}), 134.1 (q Ar, $C_{1'}$), 130.3 (CH Ar, $C_{4'}$), 130.2 (CH Ar, C_1), 128.9 (CH Ar, $C_{3'}$), 128.7 (CH Ar, C_8), 128.3 (CH Ar, C_6), 126.8 (CH Ar, $C_{2'}$), 126.8 (q Ar, C_9), 125.7 (CH Ar, C_5), 123.9 (CH Ar, C_7), 120.4 (q Ar, C_2), 110.6 (CH Ar, C_4) ppm. HRMS: $C_{18}H_{15}N_2O_2$ $[M + H]^+$ requires (m/e) 291.1134, found 291.1141.

4.3. Biological Assays. TR-FRET AR Coactivator Assay kit was used to screen for AR binders following the manufacturer's protocol.[35] In brief, serial dilutions of each compound were prepared in 100× DMSO and then diluted in coregulator buffer A to achieve 1% DMSO concentration in the plate. TR-FRET signal was measured with apppropiate

equipment using a optic module excitation 335 nm, emission 520 nm-channel A and 495 nm-channel B.

TR-FRET values were calculated at 10 flashes per well, using a delay time of 100 μs and integration time 200 μs as recommended by the Invitrogen assay guidelines. The ratio 520/495 nm was then calculated and plotted against the concentration. A 10 μL porting of compound solution was added to a 384 black well plate, following addition of 5 μL 4x AR-LBD and 5 μL of D11-FxxLF/Tb Anti-GST antibody in agonist mode and 5 μL of D11-FxxLF/Tb anti-GST antibody/DHT (included at a concentration equal to EC_{80} as determined by running the assay in agonist mode first).

$$EC_{80} = 10^{[(\log EC_{50}) + ((1/\text{hill slope}) \times \log(80/(100-80)))]}$$

D11-FxxLF and Tb antibody were premixed in light protected vials just prior to use. A final concentration of DTT 5 mM was used in the assay buffer in order to prevent protein degradation. All plates (agonist and antagonist mode) were incubated between 2 and 4 h at room temperature protected from light prior to TR-FRET measurement. IC_{50} values were determined by testing each ligand at concentrations ranging from 100 μM to 45 nM using 2-fold and 3-fold dilutions to generate a 12 point dose response curve.

Data was fitted using the sigmoidal dose response (variable slope) available from Graphpad Prism 5.[36]

$$Y = \text{bottom} + (\text{top} - \text{bottom})/(1 + 10^{[(\log IC_{50} - X)\text{hill slope})]})$$

In line with the assay protocol, a known agonist, dihydrotestosterone (DHT, cat no. A8380, Sigma) and a known antagonist, cyproterone acetate (cat no. C3412, Sigma), were used as controls. A control with no AR-LBD present was included to account for diffusion enhanced FRET or ligand-independent coactivator recruitment. A negative control with 2× DMSO was present to account for any solvent vehicle effects.

4.4. Crystallographic Data of Compound 2a. Cambridge Database Deposition number: CCDC 864271, $C_{44}H_{32}N_4O_4$, M = 680.74, monoclinic, a = 15.352(3), b = 6.4600(13), c = 8.4600(17) Å, α = 90°, β = 91.48(3)°, γ = 90°, U = 838.7(3)Å^3, T = 123 K, space group Pc, Z = 1, μ (Mo Kα) = 0.09 mm^{-1}, ρ = 1.348 g cm^{-3}, 12 088 reflections collected, 2680 unique, (R_{int} = 0.0654), $^aR_1$ = 0.1855, wR_2 [$I > 2\sigma(I)$] = 0.5210, Gof = 2.164, $^aR_1 = \sum||F_o| - |F_c||/\sum|F_o|$, $wR_2 = [\sum w(F_o^2 - F_c^2)^2/\sum w(F_o^2)^2]^{1/2}$.

5. COMPUTATIONAL DETAILS

The systems have been optimized by the Gaussian-09 package[37] using the B3LYP[38,39] functional with the 6-311++G(d,p)[40] basis set. Frequency calculations have been performed to confirm that the resulting optimized structures are energetic minima. Effects of water solvation have been included by means of the SCRF-PCM[41] approaches implemented in Gaussian-09.

■ ASSOCIATED CONTENT

Supporting Information

Supporting Information associated with this article includes ^{1}H NMR, ^{13}C NMR, and NOE spectra, crystallographic data, calculated absolute energies, and Cartesian coordinates of optimized structures. This material is available free of charge via Internet at http://pubs.acs.org.

■ AUTHOR INFORMATION

Corresponding Author

*Tel: +353-1-896 2304. Fax: +353-1-896 2303. E-mail: lloyddg@tcd.ie (D.G.L.); blancof@tcd.ie (F.B.).

Notes

The authors declare no competing financial interest.

■ ACKNOWLEDGMENTS

This work has been funded by the Health Research Board (HRB/2007/2) and the European Commission (Marie-Curie grant, People FP7, Project Reference: 274988). The Trinity Biomedical Sciences Institute is supported a capital infrastructure investment from Cycle 5 of the Irish Higher Education Authority's Programme for Research in Third Level Institutions (PRTLI). Calculations were performed on the Stokes cluster maintained by the Irish Centre for High-End Computing (ICHEC). We would like to thank Dr Martin Peters for his assistance.

■ REFERENCES

(1) Caboni, L.; Kinsella, G. K.; Blanco, F.; Fayne, D.; Jagoe, W. N.; Carr, M.; Williams, D. C.; Meegan, M. J.; Lloyd, D. True" Antiandrogens—Selective Non-Ligand-Binding Pocket Disruptors of Androgen Receptor−Coactivator Interactions: Novel Tools for Prostate Cancer. *J. Med. Chem.* **2012**, *55* (4), 1635−1644.

(2) Evans, R. M. The steroid and thyroid hormone receptor superfamily. *Science* **1988**, *240*, 889−895.

(3) Bain, D. L.; Heneghan, A. F.; Connaghan-Jones, K. D.; Miura, M. T. Nuclear receptor structure: implications for function. *Annu. Rev. Physiol.* **2007**, *69*, 201−220.

(4) Karabatsos, G. J.; Graham, J. D.; Vane, F. M. Syn-anti Isomer Determination of 2,4-Dinitrophenylhydrazones and Semicarbazones by N.M.R. *J. Am. Chem. Soc.* **1962**, *84*, 753−755.

(5) Karabatsos, G. J.; Shapiro, B. L.; Fleming, J. S.; Ratka, J. S. Structural Studies by Nuclear Magnetic Resonance. II. Aldehyde 2,4-Dinitrophenylhydrazones. *J. Am. Chem. Soc.* **1963**, *85*, 2784−2788.

(6) Karabatsos, G. J.; Taller, R. A. Structural Studies by Nuclear Magnetic Resonance. V. Phenylhydrazones. *J. Am. Chem. Soc.* **1963**, *85*, 3624−3629.

(7) Karabatsos, G. J.; Vane, F. M.; Taller, R. A.; Hsi, N. Structural studies by nuclear magnetic resonance. VIII. Ring-Substituted Phenylhydrazones, Semicarbazones, and Thiosemicarbazones. *J. Am. Chem. Soc.* **1964**, *86*, 3351−3357.

(8) Karabatsos, G. J.; Hsi, N. Structural studies by nuclear magnetic resonance-XI: Conformations and configurations of oxime o-methyl ethers. *Tetrahedron* **1967**, *23*, 1079−1095.

(9) Karabatsos, G. J.; Lande, S. S. Structural studies by nuclear magnetic resonance-XVIII: Conformational and configurational isomerism of N-alkyl imines. *Tetrahedron* **1968**, *24*, 3907−3922.

(10) Karabatsos, G. J.; Taller, R. A. Structural studies by nuclear magnetic resonance-XV: Conformations and configurations of oximes. *Tetrahedron* **1968**, *24*, 3347−3360.

(11) Karabatsos, G. J.; Taller, R. A. Structural studies by nuclear magnetic resonance-XVII: Conformations and configurations of N-methylhydrazones. *Tetrahedron* **1968**, *24*, 3557−3568.

(12) Karabatsos, G. J.; Osborne, C. E. Structural studies by nuclear magnetic resonance-XVI: Conformations and configurations of hydrazones. *Tetrahedron* **1968**, *24*, 3361−3368.

(13) Stassinopoulou, C. I.; Zioudrou, C.; Karabatsos, G. J. Temperature dependence of the C-methyl chemical shifts in N-substituted hydrazones of acetone. *Tetrahedron Lett.* **1972**, *13*, 3671−3674.

(14) Stassinopoulou, C. I.; Zioudrou, C.; Karabatsos, G. J. Solvent effects on the syn-anti isomerization rates of hydrazones of acetone. *Tetrahedron* **1976**, *32*, 1147−1151.

(15) Minabe, M.; Takabayashi, Y.; Setta, Y.; Nakamura, H.; Kimura, T.; Tsubota, M. Characterization of 9-(p-Substituted Benzylidenehydrazono)fluorenes. *Bull. Chem. Soc. Jpn.* **1996**, *69*, 3633−3638.
(16) Ramanathan, S.; Lemal, D. M. Conformational and configurational dynamics of a highly fluorinated hydrazone. *J. Org. Chem.* **2007**, *72*, 1566−1569.
(17) Blanco, F.; Alkorta, I.; Elguero, J. Barriers about Double Carbon-Nitrogen Bond in Imine Derivatives Aldimines, Oximes, Hydrazones, Azines). *Croat. Chim. Acta* **2009**, *82*, 173−183.
(18) Chapelle, J. P.; Elguero, J.; Jacquier, R.; Tarrago, G. Studies on enehydrazines 2. Reaction of trimethylhydrazine with ketones − Formation of enehydrazines and *N,N*-dimethylhydrazones. *Bull. Soc. Chim. Fr.* **1970**, 3145−3146.
(19) Lu, S. I. Gibbs energy of activation for thermal isomerization of (1Z)-acetaldehyde hydrazone and (1Z)-acetaldehyde N,N-dimethylhydrazone by Gaussian-4 theory and CCSD(T)/CBS computations. *J. Comput. Chem.* **2009**, *30*, 2176−2180.
(20) Trabelsi, M.; Salem, M.; Champagne, B. Investigation of the configuration of alkyl phenyl ketone phenylhydrazones from ab initio 1H NMR chemical shifts. *Org. Biomol. Chem.* **2003**, *1*, 3839−3844.
(21) Langa, F.; de la Cruz, P.; Delgado, J. L.; Haley, M. M.; Shirtcliff, L.; Alkorta, I.; Elguero, J. The structure of p-nitrophenylhydrazones of aldehydes: the case of the p-nitrophenylhydrazone of 2-diethylamino-5-methoxy-2H-indazole-3-carboxaldehyde. *J. Mol. Struct.* **2004**, *699*, 17−21.
(22) Savini, L.; Chiasserini, L.; Gaeta, A.; Pellerano, C. Synthesis and anti-tubercular evaluation of 4-quinolylhydrazones. *Bioorg. Med. Chem.* **2002**, *10*, 2193−2198.
(23) Wyrzykiewicz, E.; Prukala, D. New Isomeric N-substituted Hydrazones of 2-, 3- and 4-Pyridinecarboxaldehydes. *J. Heterocycl. Chem.* **1998**, *35*, 381−387.
(24) Brokaite, K.; Mickevicius, V.; Mikulskiene, G. Synthesis and structural investigation of some 1,4-disubstituted-2-pyrrolidinones. *Arkivoc* **2006**, *ii*, 61−67.
(25) Kuodis, Z.; Rutavicius, A.; Matijoska, A.; Eicher-Lorka, O. Synthesis and isomerism of hydrazones of 2-(5-thioxo-4,5-dihydro-1,3,4-thiadiazol-2-ylthio)acetohydrazide. *Centr. Eur. J. Chem.* **2007**, *5*, 996−1006.
(26) Ershov, A. Y.; Lagoda, I. V.; Yakimovich, S. I.; Pakal'nis, V. V.; Zerova, I. V.; Dobrodumov, A. V.; Shamanin, V. V. Tautomerism and conformational isomerism of mercaptoacetylhydrazones of aliphatic and aromatic aldehydes. *Russ. J. Org. Chem.* **2009**, *45*, 660−666.
(27) Monfared, H. H.; Bikas, R.; Mayer, P. (E)-3-Hydroxy-N′-(2-hydroxybenzylidene)-2-naphthohydrazide. *Acta Crystallogr. (E)* **2010**, *66*, o236−o237.
(28) Cambridge Crystallographic Data Centre (CCDC), 12 Union Road, Cambridge CB2 1EZ, England.
(29) Pope, A. J.; Haupts, U. M.; Moore, K. J. Homogeneous fluorescence readouts for miniaturized high-throughput screening: theory and practice. *Drug Discov. Today.* **1999**, *4*, 350−362.
(30) Gunther, J. R.; Du, Y.; Rhoden, E.; Lewis, I.; Revennaugh, B.; Moore, T. W.; Kim, S. H.; Dingledine, R.; Fu, H.; Katzenellenbogen, J. A. A set of time-resolved fluorescence resonance energy transfer assays for the discovery of inhibitors of estrogen receptor-coactivator binding. *J. Biomol. Screen* **2009**, *14*, 181−193.
(31) Compounds **2a−c** and **3** were synthesized according to the procedure described, all the other compounds evaluated in the biological studies were purchased from the company Specs (http://www.specs.net).
(32) Razniewska-Lazecka, G. ^{13}C NMR spectra of some o-carbonyl derivatives of naphthols. *Magn. Reson. Chem.* **1986**, *24* (4), 365−367.
(33) Karpagam, J. Molecular structure, vibrational spectroscopic, first-order hyperpolarizability and HOMO, LUMO studies of 3-hydroxy-2-naphthoic acid hydrazide. *J. Raman Spectrosc.* **2010**, *41* (1), 53−62.
(34) Pant, U. C.; Ramchandran, R.; Joshi, B. C. Studies on 1-hydroxy-2-naphtoic and 3-hydroxy-2-naphtoic acid hydrazides. *Rev. Roum. de Chim* **1979**, *24* (3), 471−482.
(35) TR-FRET AR Coactivator Assay kit Manual. http://tools.invitrogen.com/content/sfs/manuals/lanthascreen_AR.pdf (accessed Aug 2012).
(36) *GraphPad Prism*, version 5 for Windows; GraphPad Software, La Jolla, CA; www.graphpad.com (accessed Aug 10, 2012).
(37) Frisch, M. J.; Trucks, G. W.; Schlegel, H. B.; Scuseria, G. E.; Robb, M. A.; Cheeseman, J. R.; Scalmani, G.; Barone, V.; Mennucci, B.; Petersson, G. A.; Nakatsuji, H.; Caricato, M.; Li, X.; Hratchian, H. P.; Izmaylov, A. F.; Bloino, J.; Zheng, G.; Sonnenberg, J. L.; Hada, M.; Ehara, M.; Toyota, K.; Fukuda, R.; Hasegawa, J.; Ishida, M.; Nakajima, T.; Honda, Y.; Kitao, O.; Nakai, H.; Vreven, T.; Montgomery, Jr., J. A.; Peralta, J. E.; Ogliaro, F.; Bearpark, M.; Heyd, J. J.; Brothers, E.; Kudin, K. N.; Staroverov, V. N.; Kobayashi, R.; Normand, J.; Raghavachari, K.; Rendell, A.; Burant, J. C.; Iyengar, S. S.; Tomasi, J.; Cossi, M.; Rega, N.; Millam, N. J.; Klene, M.; Knox, J. E.; Cross, J. B.; Bakken, V.; Adamo, C.; Jaramillo, J.; Gomperts, R.; Stratmann, R. E.; Yazyev, O.; Austin, A. J.; Cammi, R.; Pomelli, C.; Ochterski, J. W.; Martin, R. L.; Morokuma, K.; Zakrzewski, V. G.; Voth, G. A.; Salvador, P.; Dannenberg, J. J.; Dapprich, S.; Daniels, A. D.; Farkas, Ö.; Foresman, J. B.; Ortiz, J. V.; Cioslowski, J.; Fox, D. J. *Gaussian 09*, Revision A.1, Gaussian, Inc.: Wallingford CT, 2009.
(38) Becke, A. D. Density-functional thermochemistry. III. The role of exact exchange. *J. Chem. Phys.* **1993**, *98*, 5648−5652.
(39) Lee, C.; Yang, W.; Parr, R. G. Development of the Colle-Salvetti correlation-energy formula into a functional of the electron density. *Phys. Rev. B* **1988**, *37*, 785−789.
(40) Frisch, M. J.; Pople, J. A.; Krishnam, R.; Binkley, J. S. Self-Consistent Molecular Orbital Methods. 25. Supplementary Functions for Gaussian Basis Sets. *J. Chem. Phys.* **1984**, *80*, 3265−3269.
(41) Tomasi, J.; Mennucci, B.; Cammi, R. Quantum mechanical continuum solvation models. *Chem. Rev.* **2005**, *105*, 2999−3093.